*Inorg. Chem.* **2005**, *44*, 6579–6590

# Heterometallic $M^{II}Ru^{III}_2$ Compounds Constructed from *trans*-$[Ru(Salen)(CN)_2]^-$ and *trans*-$[Ru(Acac)_2(CN)_2]^-$. Synthesis, Structures, Magnetic Properties, and Density Functional Theoretical Study

**Wai-Fun Yeung,[†] Pui-Ha Lau,[†] Tai-Chu Lau,*[,†] Hai-Yan Wei,[‡] Hao-Ling Sun,[‡] Song Gao,*[,‡] Zhi-Da Chen,*[,‡] and Wing-Tak Wong[§]**

*Department of Biology and Chemistry, City University of Hong Kong, Tat Chee Avenue, Kowloon Tong, Hong Kong, China, State Key Laboratory of Rare Earth Materials Chemistry and Applications, College of Chemistry and Molecular Engineering, Peking University, Beijing 100871, China, and Department of Chemistry, The University of Hong Kong, Pokfulam Road, Hong Kong, China*

Received April 27, 2005

The synthesis, structures, and magnetic properties of four cyano-bridged $M^{II}Ru^{III}_2$ compounds prepared from the paramagnetic $Ru^{III}$ building blocks, *trans*-$[Ru(salen)(CN)_2]^-$ **1** [$H_2$salen = *N*,*N*′-ethylenebis(salicylideneimine)] and *trans*-$[Ru(acac)_2(CN)_2]^-$ (Hacac = acetylacetone), are described. Compound **2**, $\{Mn(CH_3OH)_4[Ru(salen)(CN)_2]_2\}\cdot 6CH_3OH\cdot 2H_2O$, is a trinuclear complex that exhibits antiferromagnetic coupling between $Mn^{II}$ and $Ru^{III}$ centers. Compound **3**, $\{Mn(H_2O)_2[Ru(salen)(CN)_2]_2\cdot H_2O\}_n$, has a 2-D sheetlike structure that exhibits antiferromagnetic coupling between Mn and Ru, leading to ferrimagnetic-like behavior. Compound **4**, $\{Ni(cyclam)[Ru(acac)_2(CN)_2]_2\}\cdot 2CH_3OH\cdot 2H_2O$ (cyclam = 1,4,8,11-tetraazacyclotetradecane), is a trinuclear complex that exhibits ferromagnetic coupling. Compound **5**, $\{Co[Ru(acac)_2(CN)_2]_2\}_n$, has a 3-D diamond-like interpenetrating network that exhibits ferromagnetic ordering below 4.6 K. The density functional theory (DFT) method was used to calculate the molecular magnetic orbitals and the magnetic exchange interaction between $Ru^{III}$ and $M^{II}$ ($Mn^{II}$, $Ni^{II}$) ions.

## Introduction

Hexacyanometalates, $[M(CN)_6]^{n-}$, have long been used as building blocks in conjunction with 3d ions to produce a number of Prussian Blue type (PB) compounds.[1] Some of these PB type compounds, such as V−Cr cyanide systems, are of particular interest since they exhibit bulk magnetization at high temperatures.[1f,h,i] Owing to the high symmetry of the metal sites in PB compounds, the nature of the interaction between 3d magnetic orbitals is usually governed by symmetry rules.[1,2] The preparation of molecule-based magnetic materials using paramagnetic 4d and 5d metal ions has received more attention in recent years since their orbitals are more diffuse, and so enhanced magnetic interactions may be expected. In addition, the use of lower symmetry 4d/5d building blocks, such as $[Mo^{III}(CN)_7]^{4-}$, could allow one to study the effects of anisotropy on magnetic properties.[3]

We note that examples of 3d−4d and 3d−5d coordination polymers in the field of molecular magnetism are mostly constructed from precursors such as $[Mo^{III}(CN)_7]^{4-}$,[3a−f,4] $[M^{IV/V}(CN)_8]^{4/3-}$ (M = $Mo^{IV/V}$, $W^{IV/V}$ and $Nb^{IV}$),[5] $[Ru^{III}(ox)_3]^{3-}$ (ox = oxalato),[6] and $[Re^{II}(triphos)(CN)_3]^-$.[7] The symmetry rule seems to be invalid for a few compounds, for example, the nature of the magnetic interaction in $(Bu_4N)[Mn^{II}Ru^{III}$-

* Authors to whom correspondence should be addressed. E-mail: bhtclau@cityu.edu.hk (T.-C.L.); gaosong@pku.edu.cn (S.G.); zdchen@pku.edu.cn (Z.-D.C.).

† City University of Hong Kong.

‡ Peking University.

§ The University of Hong Kong.

(1) For example (a) Gadet, V.; Mallah, T.; Castro, I.; Verdaguer, M.; Veillet, P. *J. Am. Chem. Soc*. **1992**, *114*, 9213−9214. (b) Mallah, T.; Thiébaut, S.; Verdaguer, M.; Veillet, P. *Science* **1993**, *262*, 1554−1557. (c) Entley, W. R.; Girolami, G. S. *Inorg. Chem.* **1994**, *33*, 5165−5166. (d) Entley, W. R.; Girolami, G. S. *Science* **1995**, *268*, 397−400. (e) Kahn, O. *Nature* **1995**, *378*, 667−668. (f) Ferlay, S.; Mallah, T.; Ouahes, R.; Veillet, P.; Verdaguer, M. *Nature* **1995**, *378*, 701−703. (g) Verdaguer, M. *Science* **1996**, *272*, 698−699. (h) Hatlevik, Ø; Buschmann, W. E.; Zhang, J.; Manson, J. L.; Miller, J. S. *Adv. Mater*. **1999**, *11*, 914−918. (i) Holmes, S. M.; Girolami, G. S. *J. Am. Chem. Soc*. **1999**, *121*, 5593−5594.

(2) Verdaguer, M.; Bleuzen, A.; Marvaud, V.; Vaissermann, J.; Seuleiman, M.; Desplanches, C.; Scuiller, A.; Train, C.; Garde, R.; Gelly, G.; Lomenech, C.; Rosenman, I.; Veillet, P.; Cartier, C.; Villain, F. *Coord. Chem. Rev.* **1999**, *190*, 1023−1047.

10.1021/ic0506456 CCC: $30.25 
Published on Web 08/11/2005

$(ox)_3$] is ferromagnetic, while that in $(Bu_4N)[Cu^{II}Ru^{III}(ox)_3]$ is antiferromagnetic.[6] Moreover, the magnetic behavior of a number of $Mo^{III}-C\equiv N-Mn^{II}$ compounds, such as $Mn_2(H_2O)_5Mo(CN)_7\cdot 4H_2O$ ($\alpha$-phase),[3c] $K_2Mn_3(H_2O)_6[Mo(CN)_7]_2\cdot 6H_2O$,[3d] and $Mn_2(H_2O)_5[Mo(CN)_7]\cdot 4.75H_2O$ ($\beta$-phase),[3e] is unusual in that the Weiss constant is positive based on the magnetic susceptibility data in the high-temperature range, but the coupling between $Mo^{III}-Mn^{II}$ is antiferromagnetic.[3h] To gain insight into the nature of the magnetic interaction between 4d/5d and 3d paramagnetic centers, more systematic investigation involving both experimental and theoretical work is required.

We are interested in constructing magnetic materials based on ruthenium(III) and osmium(III) centers. There are a number of coordination polymers constructed from $[Ru^{III}(ox)_3]^{3-}$; however, they have not been structurally characterized.[6] We recently reported a new dicyanoruthenate(III) building block, *trans*-$[Ru(acac)_2(CN)_2]^-$ (Hacac = acetylacetone). Reaction of this building block with $Mn^{2+}$ produces a novel 3-D cyano-bridged $Ru^{III}_2Mn^{II}$ compound, $\{Mn[Ru(acac)_2(CN)_2]\}_n$, which has a diamond-like structure and exhibits ferromagnetic ordering at low temperatures.[8] This is the first structurally characterized coordination polymer that contains Ru(III). To gain more insight into the nature of the magnetic interaction between Ru(III) and 3d paramagnetic centers, we have designed several other $Ru^{III}_2M^{II}$ compounds based on the paramagnetic $Ru^{III}$ building blocks *trans*-$[Ru(salen)(CN)_2]^-$ **1** [$H_2$salen = *N*,*N*′-ethylenebis(salicylideneimine)] and *trans*-$[Ru(acac)_2(CN)_2]^-$. We report here the synthesis, structures, and magnetic properties of trinuclear $\{Mn(CH_3OH)_4[Ru(salen)(CN)_2]_2\}\cdot 6CH_3OH\cdot 2H_2O$ **2**, 2-D $\{Mn(H_2O)_2[Ru(salen)(CN)_2]_2\cdot H_2O\}_n$ **3**, trinuclear $\{Ni(cyclam)[Ru(acac)_2(CN)_2]_2\}\cdot 2CH_3OH\cdot 2H_2O$ **4** (cyclam = 1,4,8,11-tetraazacyclotetradecane), and 3-D $\{Co[Ru(acac)_2(CN)_2]_2\}_n$ **5**.

The density functional theory (DFT) method was used to calculate the molecular magnetic orbitals and the magnetic exchange interaction between $Ru^{III}$ and $M^{II}$ ($Mn^{II}$, $Ni^{II}$) ions. The availability of a series of $Ru^{III}_2Mn^{II}$ compounds with different structures, including trinuclear, 2-D, and 3-D,[8] gives us an opportunity to investigate the magneto-structural correlation between these paramagnetic centers.

## Experimental Procedures

**Measurements.** Elemental analyses were carried out using an Elementar vario EL CHN analyzer. The IR spectra were recorded as KBr disks on a Perkin-Elmer FTIR-1600 and a Bomen MB-120 FTIR spectrophotometer in the 4000−400 $cm^{-1}$ region. Electrospray ionization mass spectra were recorded on a SCIEX API 365 quadrupole mass spectrometer. Magnetic measurements were performed on either a Maglab 2000 System or a MPMS-XL-5 SQUID magnetometer. The experimental susceptibilities were corrected for the diamagnetism of the constituent atoms (Pascal's tables).

**Preparations.** All chemicals and reagents were commercially available and used as received. *trans*-$Ph_4P[Ru(Acac)_2(CN)_2]$[8] and $Mn(acac)_3$[9] were synthesized according to literature methods.

**Caution:** Perchlorate salts of metal complexes with organic ligands are potentially explosive and should be handled in small quantities with care.

**Preparation of *trans*-$Bu_4N[Ru(Salen)(CN)_2]$ (1).** This compound was prepared according to the literature.[10] Crystals suitable for X-ray crystallography were obtained by slow diffusion of diethyl ether into a solution of **1** in methanol. IR (KBr/$cm^{-1}$): $\nu_{CN}$ 2096 (s).


(3) (a) Larionova, J.; Sanchiz, J.; Golhen, S.; Ouahab, L.; Kahn, O. *Chem. Commun.* **1998**, 953−954. (b) Sra, A. K.; Andruh, M.; Kahn, O.; Golhen, S.; Ouahab, L.; Yakhmi, J. V. *Angew. Chem., Int. Ed.* **1999**, *38*, 2606−2609 and *Angew. Chem.* **1999**, *111*, 2768−2771. (c) Larionova, J.; Clérac, R.; Sanchiz, J.; Kahn, O.; Golhen, S.; Ouahab, L. *J. Am. Chem. Soc.* **1998**, *120*, 13088−13095. (d) Larionova, J.; Kahn, O.; Golhen, S.; Ouahab, L.; Clérac, R. *J. Am. Chem. Soc.* **1999**, *121*, 3349−3356. (e) Larionova, J.; Kahn, O.; Golhen, S.; Ouahab, L.; Clérac, R. *Inorg. Chem.* **1999**, *38*, 3621−3627. (f) Larionova, J.; Clérac, R.; Donnadieu, B.; Guérin, C. *Chem.—Eur. J.* **2002**, *8*, 2712−2716. (g) Mironov, V. S.; Chibotaru, L. F.; Ceulemans, A. *J. Am. Chem. Soc.* **2003**, *125*, 9750−9760. (h) Larionova, J.; Willemin, S.; Donnadieu, B.; Henner, B.; Guérin, C.; Gillon, B.; Goujon, A. *J. Phys. Chem. Sol.* **2004**, *65*, 677−691.

(4) (a) Tanase, S.; Tuna, F.; Guionneau, P.; Maris, T.; Rombaut, G.; Mathonière, C.; Andruh, M.; Kahn, O.; Sutter, J.-P. *Inorg. Chem.* **2003**, *42*, 1625−1631. (b) Le Goff, X. F.; Willemin, S.; Coulon, C.; Larionova, J.; Donnadieu, B.; Clérac, R. *Inorg. Chem.* **2004**, *43*, 4784−4786.

(5) (a) Sra, A. K.; Rombaut, G.; Lahitête, F.; Golhen, S.; Ouahab, L.; Mathonière, C.; Yakhmi, J. V.; Kahn, O. *New J. Chem.* **2000**, *24*, 871−876. (b) Rombaut, G.; Golhen, S.; Ouahab, L.; Mathonière, C.; Kahn, O. *J. Chem. Soc., Dalton Trans.* **2000**, 3609−3614. (c) Zhong, Z. J.; Seino, H.; Mizobe, Y.; Hidai, M.; Verdaguer, M.; Ohkoshi, S.-i.; Hashimoto, K. *Inorg. Chem.* **2000**, *39*, 5095−5101. (d) Rombaut, G.; Mathonière, C.; Guionneau, P.; Golhen, S.; Ouahab, L.; Verelst, M.; Lecante, P. *Inorg. Chim. Acta* **2001**, *326*, 27−36. (e) Rombaut, G.; Verelst, M.; Golhen, S.; Ouahab, L.; Mathonière, C.; Kahn, O. *Inorg. Chem.* **2001**, *40*, 1151−1159. (f) Chibotaru, L. F.; Mironov, V. S.; Ceulemans, A. *Angew. Chem., Int. Ed.* **2001**, *40*, 4429−4433 and *Angew. Chem.* **2001**, *113*, 4561−4565. (g) Arimoto, Y.; Ohkoshi, S.-i.; Zhong, Z. J.; Seino, H.; Mizobe, Y.; Hashimoto, K. *Chem. Lett.* **2002**, 832−833. (h) Li, D.-F.; Gao, S.; Zheng, L.-M.; Sun, W.-Y.; Okamura, T.-a.; Ueyama, N.; Tang, W.-X. *New J. Chem.* **2002**, *26*, 485−489. (i) Li, D.-F.; Gao, S.; Zheng, L.-M.; Yu, K.-B.; Tang, W.-X. *New J. Chem.* **2002**, *26*, 1190−1195. (j) Li, D.-F.; Gao, S.; Zheng, L.-M.; Tang, W.-X. *J. Chem. Soc., Dalton Trans.* **2002**, 2805−2806. (k) Podgajny, R.; Korzeniak, T.; Balanda, M.; Wasiutynski, T.; Errington, W.; Kemp, T. J.; Alcock, N. W.; Sieklucka, B. *Chem. Commun.* **2002**, 1138−1139. (l) Korzeniak, T.; Podgajny, R.; Alcock, N. W.; Lewiñski, K.; Ba_anda, M.; Wasiutyñski, T.; Sieklucka, B. *Polyhedron* **2003**, *22*, 2183−2190. (m) Li, D.-F.; Zheng, L.-M.; Wang, X.-Y.; Huang, J.; Gao, S.; Tang, W.-X. *Chem. Mater.* **2003**, *15*, 2094−2098. (n) Ohkoshi, S.-i.; Arimoto, Y.; Hozumi, T.; Seino, H.; Mizobe, Y.; Hashimoto, K. *Chem. Commun.* **2003**, 2772−2773. (o) Song, Y.; Ohkoshi, S.-i.; Arimoto, Y.; Seino, H.; Mizobe, Y.; Hashimoto, K. *Inorg. Chem.* **2003**, *42*, 1848−1856. (p) Li, D.-F.; Zheng, L.-M.; Zhang, Y.-Z.; Huang, J.; Gao, S.; Tang, W.-X. *Inorg. Chem.* **2003**, *42*, 6123−6129. (q) Pradhan, R.; Desplanches, C.; Guionneau, P.; Sutter, J.-P. *Inorg. Chem.* **2003**, *42*, 6607−6609. (r) Herrera, J. M.; Bleuzen, A.; Dromzée, Y.; Julve, M.; Lloret, F.; Verdaguer, M. *Inorg. Chem.* **2003**, *42*, 7052−7059. (s) Arimoto, Y.; Ohkoshi, S.-i.; Zhong, Z.-J.; Seino, H.; Mizobe, Y.; Hashimoto, K. *J. Am. Chem. Soc.* **2003**, *125*, 9240−9241. (t) Kou, H.-Z.; Ni, Z.-H.; Zhou, B. C.; Wang, R.-J. *Inorg. Chem. Commun.* **2004**, *7*, 1150−1153. (u) Kou, H.-Z.; Zhou, B.-C.; Si, S.-F.; Wang, R.-J. *Eur. J. Inorg. Chem.* **2004**, 401−408. (v) Przychodzeñ, P.; Lewiñski, K.; Balanda, M.; Pelka, R.; Rams, M.; Wasiutyñski, T.; Guyard-Duhayon, C.; Sieklucka, B. *Inorg. Chem.* **2004**, *43*, 2967−2974. (w) Korzeniak, T.; Stadnicka, K.; Rams, M.; Sieklucka, B. *Inorg. Chem.* **2004**, *43*, 4811−4813. (x) Kashiwagi, T.; Ohkoshi, S.-i.; Seino, H.; Mizobe, Y.; Hashimoto, K. *J. Am. Chem. Soc.* **2004**, *126*, 5024−5025. (y) Song, Y.; Zhang, P.; Ren, X.-M.; Shen, X.-F.; Li, Y.-Z.; You, X.-Z. *J. Am. Chem. Soc.* **2005**, *127*, 3708−3709.

(6) Larionova, J.; Mombelli, B.; Sanchiz, J.; Kahn, O. *Inorg. Chem.* **1998**, *37*, 679−684.

(7) Schelter, E. J.; Prosvirin, A. V.; Dunbar, K. R. *J. Am. Chem. Soc.* **2004**, *126*, 15004−15005.

(8) Yeung, W.-F.; Man, W.-L.; Wong, W.-T.; Lau, T.-C.; Gao, S. *Angew. Chem., Int. Ed.* **2001**, *40*, 3031−3033 and *Angew. Chem.* **2001**, *113*, 3121−3123.

(9) Girolami, G. S.; Rauchfuss, T. B.; Angelici, R. J. *Synthesis and Techniques in Inorganic Chemistry, A LABORATORY MANUAL*; University Science Books: Sausalito, CA, 1999.

(10) Leung, W.-H.; Che, C.-M. *Inorg. Chem.* **1989**, *28*, 4619−4622.

**Table 1.** Crystal Data for $Bu_4N[Ru(Salen)(CN)_2]$ (**1**), $Mn(CH_3OH)_4[Ru(Salen)(CN)_2]_2\cdot 6CH_3OH\cdot 2H_2O$ (**2**), $\{Mn(H_2O)_2[Ru(Salen)(CN)_2]_2\cdot H_2O\}_n$ (**3**), $Ni(Cyclam)[Ru(acac)_2(CN)_2]_2\cdot 2CH_3OH\cdot 2H_2O$ (**4**), and $\{Co[Ru(Acac)_2(CN)_2]_2\}_n$ (**5**)

| compound | **1** | **2** | **3** | **4** | **5** |
|---|---|---|---|---|---|
| chemical formula | $RuN_5C_{34}O_2H_{50}$ | $Ru_2MnN_8C_{46}O_{16}H_{72}$ | $Ru_2MnN_8C_{36}O_7H_{34}$ | $Ru_2NiN_8C_{36}O_{12}H_{64}$ | $Ru_2CoN_4C_{24}O_8H_{28}$ |
| Fw | 661.87 | 1250.20 | 947.79 | 1061.79 | 761.58 |
| cryst syst | monoclinic | monoclinic | tetragonal | triclinic | tetragonal |
| cryst dimensions [mm] | 0.02 × 0.08 × 0.45 | 0.10 × 0.18 × 0.30 | 0.32 × 0.12 × 0.12 | 0.03 × 0.06 × 0.18 | 0.48 × 0.11 × 0.10 |
| cryst syst | monoclinic | monoclinic | tetragonal | triclinic | tetragonal |
| lattice type | primitive | primitive | primitive | primitive | primitive |
| *a* [Å] | 12.051(4) | 13.4134(7) | 14.7990(9) | 7.622(1) | 13.425(2) |
| *b* [Å] | 13.227(6) | 18.1077(9) | 14.7990(9) | 11.908(1) | 13.425(2) |
| *c* [Å] | 21.673(5) | 12.8645(6) | 17.114(1) | 14.448(1) | 8.224(2) |
| α [°] | 90 | 90 | 90 | 70.41(1) | 90 |
| *β* [°] | 94.78(2) | 103.853(10) | 90 | 81.31(1) | 90 |
| *γ* [°] | 90 | 90 | 90 | 87.32(1) | 90 |
| *V* [Å$^3$] | 3442(1) | 3033.7(3) | 3748.1(3) | 1221.2(2) | 1482.2(4) |
| space group | $P2_1/c$ (No. 14) | $P2_1/c$ (No. 14) | $P4/ncc$ (No. 130) | $P\bar{1}$ (No. 2) | $P4_2/n$ (No. 86) |
| *Z* value | 4 | 2 | 4 | 1 | 2 |
| $D_{calc}$ [g cm$^{-3}$] | 1.277 | 1.369 | 1.672 | 1.444 | 1.706 |
| $F_{000}$ | 1396.00 | 1290.00 | 1884.00 | 548 | 758.00 |
| $\mu$(Mo Kα) [cm$^{-1}$] | 4.91 | 7.62 | 11.87 | 10.52 | 16.09 |
| no. of params | 299 | 355 | 124 | 253 | 90 |
| *T* [K] | 301 | 298 | 273 | 298 | 298 |
| $2\theta_{max}$ [deg] | 45 | 55 | 55 | 55.2 | 55 |
| measured reflns | 4721 | 6951 | 2516 | 5310 | 1816 |
| obsd reflns | 2374 | 6951 | 1160 | 3210 | 1430 |
| largest peak/hole [e Å$^{-3}$] | 1.09/−0.63 | 0.77/−0.31 | 1.30/−0.61 | 1.05/−0.45 | 0.63/−0.50 |
| final *R* indices | [$I > 1.50\sigma(I)$] | [$I > 2.00\sigma(I)$] | [$I > 1.50\sigma(I)$] | [$I > 1.50\sigma(I)$] | [$I > 1.50\sigma(I)$] |
| residuals: $R^a$ and $R_w{}^b$ | 0.096, 0.100 | 0.039, 0.048 | 0.051, 0.056 | 0.059, 0.064 | 0.031, 0.044 |
| GOF | 2.57 | 1.022 | 1.52 | 1.12 | 1.43 |

$^a$ $R = \sum(||F_o| - |F_c||)/\sum|F_o|$. $^b$ $R_w = [\sum\{(|F_o| - |F_c|)^2/\sum wF_o^2\}^{1/2}$.

**{Mn(CH$_3$OH)$_4$[Ru(Salen)(CN)$_2$]$_2$}·6CH$_3$OH·2H$_2$O (2).** A reaction mixture containing $Bu_4N[Ru(salen)(CN)_2]$ (66 mg, 0.1 mmol) and $Mn(acac)_3$ (36 mg, 0.1 mmol) in 15 mL of methanol was refluxed under argon for 2 h. The resulting dark green solution was left undisturbed at 4 °C for 1 month to produce dark green crystals. Yield: 21%. Anal. calcd for $Ru_2MnN_8C_{46}O_{16}H_{72}$: C, 44.19; H, 5.80; N, 8.96%. Found: C, 44.50; H, 5.62; N, 8.85%. IR (KBr/cm$^{-1}$): $\nu_{CN}$ 2115 (s).

**{Mn(H$_2$O)$_2$[Ru(Salen)(CN)$_2$]$_2$·H$_2$O}$_n$ (3).** A methanolic solution (30 mL) of $Bu_4N[Ru(salen)(CN)_2]$ (132 mg, 0.2 mmol) and $Mn(ClO_4)_2\cdot 6H_2O$ (36 mg, 0.1 mmol) was stirred for 2 days. The white precipitate formed was filtered off, and the dark green filtrate was left undisturbed for a few weeks to give dark green crystals. Yield: 30%. Anal. calcd for $Ru_2MnN_8C_{36}O_7H_{34}$: C, 45.62; H, 3.62; N, 11.82%. Found: C, 45.52; H, 4.01; N, 11.90%. IR (KBr/cm$^{-1}$): $\nu_{CN}$ 2116 (s).

**{Ni(Cyclam)[Ru(Acac)$_2$(CN)$_2$]$_2$}·2CH$_3$OH·2H$_2$O (4).** A solution of $NiCl_2\cdot 6H_2O$ (48 mg, 0.2 mmol) and cyclam (40 mg, 0.2 mmol) in 10 mL of methanol was slowly added to a solution of *trans*-$Ph_4P[Ru(acac)_2(CN)_2]$ (69 mg, 0.1 mmol) in 10 mL of methanol with rapid stirring. The solution was filtered to remove some purple precipitate, and slow evaporation of filtrate gave dark purple crystals. Yield: 52%. Anal. calcd for $Ru_2NiN_8C_{36}O_{12}H_{64}$: C, 40.72; H, 6.08; N, 10.55%. Found: C, 40.56; H, 6.06; N, 10.33%. IR (KBr/cm$^{-1}$): $\nu_{CN}$ 2118 (s).

**{Co[Ru(Acac)$_2$(CN)$_2$]$_2$}$_n$ (5).** Compound **5** was obtained by a slow diffusion method. The reactants $CoCl_2\cdot 6H_2O$ (24 mg, 0.1 mmol) and *trans*-$Ph_4P[Ru(acac)_2(CN)_2]$ (138 mg, 0.2 mmol) contained in two separate 10 mL sample tubes were placed together in a 150 mL beaker. The sample tubes and beaker were then carefully filled with methanol. Dark purple needle-shaped crystals were obtained after leaving the beaker undisturbed at room temperature for 2 weeks. Yield: 40%. Anal. calcd for $Ru_2CoN_4C_{24}O_8H_{28}$: C, 37.85; H, 3.71; N, 7.36%. Found: C, 37.65; H, 3.90; N, 7.20%. IR (KBr/cm$^{-1}$): $\nu_{CN}$ 2125 (s).

**X-ray Crystallography.** Diffraction data on a crystal of **1** were collected on a Rigaku AFC7R diffractometer with graphite monochromated Mo Kα radiation ($\lambda = 0.71069$ Å). Data on a crystal of **2**−**5** were collected on a Bruker SMART CCD diffractometer with graphite monochromated Mo Kα radiation ($\lambda = 0.71069$ Å). The diffracted intensities were corrected for Lorentz and polarization effects. Absorption corrections were also applied by SADABS.[11] The structures were solved by direct methods (SIR 92[12] for **1** and SHELXS 86[13] for **3** and **5**) and the heavy atom Patterson method[14] (PATTY, for **2** and **4**). The structures were expanded using Fourier difference techniques (DIRDIF94[15] for **1** and **3**−**5** and DIRDIF99[16] for **2**). The atomic coordinates and thermal parameters were refined by full-matrix least squares on *F*, with anisotropic displacement parameters for non-hydrogen atoms whenever possible. Hydrogen atoms were included but not refined. All calculations were performed using the TeXsan crystallographic software package.[17] Summaries of crystal data collection and refinement parameters are given in Table 1.

**DFT Calculations.** All DFT calculations were performed using the Amsterdam density functional (ADF) package, version 2004.01.[18] The frozen core approximation for the inner core electrons was

(11) Sheldrick, G. M. *SADABS Empirical Absorption Correction Program*; University of Göttingen: Göttingen, Germany, 1996.
(12) Altomare, A.; Burla, M. C.; Camalli, M.; Cascarano, M.; Giacovazzo, C.; Guagliardi, A.; Polidori, G. *J. Appl. Crystallogr.* **1994**, *27*, 435.
(13) Shedrick, G. M. SHELXS-96, Program for the Solution of Crystal Structures. In *Crystallographic Computering 3*; Sheldrick, G. M., Kruger, C., Goddard, R., Eds.; Oxford University Press: Oxford, 1985; pp 175−189.
(14) Beurskens, P. T.; Admiraal, G.; Beurskens, G.; Bosman, W. P.; Garcia-Granda, S.; Gould, R. O.; Smits, J. M. M.; Smykalla, C. *The DIRDIF program system, Technical Report of the Crystallography Laboratory*; University of Nijmegen: Nijmegen, The Netherlands, 1994.
(15) Beurskens, P. T.; Admiraal, G.; Beurskens, G.; Bosman, W. P.; Gelder, R. de; Israel, R.; Smits, J. M. M. *The DIRDIF-94 program system, Technical Report of the Crystallography Laboratory*; University of Nijmegen: Nijmegen, The Netherlands, 1994.
(16) Beurskens, P. T.; Admiraal, G.; Beurskens, G.; Bosman, W. P.; Gelder, R. de; Israel, R.; Smits, J. M. M. *The DIRDIF-99 program system, Technical Report of the Crystallography Laboratory*; University of Nijmegen: Nijmegen, The Netherlands, 1999.
(17) *TeXsan, Crystal structure analysis package*; Molecular Structure Corporation: The Woodlands, TX, 1992.

**Table 2.** Selected Bond Lengths [Å] and Bond Angles [°] for **1**

| | | | |
|---|---|---|---|
| Ru(1)−O(1) | 2.02(1) | Ru(1)−O(2) | 2.03(1) |
| Ru(1)−N(1) | 2.01(1) | Ru(1)−N(2) | 2.00(1) |
| Ru(1)−C(17) | 2.04(2) | Ru(1)−C(18) | 2.09(2) |
| N(3)−C(17) | 1.16(2) | N(4)−C(18) | 1.12(2) |
| O(1)−Ru(1)−O(2) | 95.3(4) | O(1)−Ru(1)−N(1) | 90.7(5) |
| O(1)−Ru(1)−N(2) | 173.4(6) | O(1)−Ru(1)−C(17) | 90.3(6) |
| O(1)−Ru(1)−C(18) | 91.3(6) | O(2)−Ru(1)−N(1) | 173.5(5) |
| O(2)−Ru(1)−N(2) | 90.9(6) | O(2)−Ru(1)−C(17) | 90.1(6) |
| O(2)−Ru(1)−C(18) | 89.6(6) | N(1)−Ru(1)−N(2) | 83.1(6) |
| N(1)−Ru(1)−C(17) | 87.5(6) | N(1)−Ru(1)−C(18) | 92.6(7) |
| N(2)−Ru(1)−C(17) | 91.9(6) | N(2)−Ru(1)−C(18) | 86.5(6) |
| C(17)−Ru(1)−C(18) | 178.3(7) | Ru(1)−C(17)−N(3) | 178(1) |
| Ru(1)−C(18)−N(4) | 176(1) | | |

used for all non-hydrogen atoms. Orbitals up to 3d for Ru, up to 2p for Mn and Ni, and up to 1s for C, N, and O were kept frozen. A triple-$\varsigma$ valence plus polarization basis set (TZP) was used to describe the valence orbitals.

Previous reports[19] indicated that correct prediction of magnetic coupling constants when using the DFT-BS method depends on the particular exchange and correlation functionals used. In general, the agreement between the calculated and the experimental $J$ values increases in the order LDA < GGA < metaGGA < hybrid-GGA. In this work, a series of exchange correlation functionals was examined, where the local density approximation (LDA) of VWN5 functionals[20] and the various generalized gradient approximation (GGA) was used, including the scaled-ZORA relativistic correction. From our inspection, it appears that on the bases of orbitals and density from mPW-GGA,[21,22] the hybrid-B3LYP[18] functionals are the best ones. To analyze magnetic exchange interactions, the broken symmetry approach (BS)[23] within DFT was used to calculate the broken symmetry states with antiferromagnetic configuration, through the flip spin density on one spin center. Thus, the local magnetic orbital and magnetic exchange constants $J$ [$H = -2J(S_M S_{Ru1} + S_M S_{Ru2})$] can be evaluated. The details of calculation on the exchange constants have been described elsewhere.[24]

The electronic structures for the complete structures of compounds **2** and **4** were calculated by using DFT-BS. The calculation of the overlap integrals between the local magnetic orbitals on $Ru^{III}$ and $Mn^{II}$ were performed by using a program written by Chen's group.[25]

## Results and Discussion

**Synthesis, Characterizations, and Structures.** Selected bond lengths and bond angles for compounds **1**−**5** are given in Tables 2−6, respectively.

**Table 3.** Selected Bond Lengths [Å] and Bond Angles [°] for **2**

| | | | |
|---|---|---|---|
| Ru(1)−O(1) | 2.011(3) | Ru(1)−O(2) | 2.029(3) |
| Ru(1)−N(3) | 2.004(4) | Ru(1)−N(4) | 2.000(4) |
| Ru(1)−C(1) | 2.060(5) | Ru(1)−C(2) | 2.061(5) |
| Mn(2)−O(3) | 2.191(5) | Mn(2)−O(4) | 2.205(4) |
| Mn(2)−N(2) | 2.155(4) | N(1)−C(1) | 1.143(7) |
| N(2)−C(2) | 1.147(7) | | |
| O(1)−Ru(1)−O(2) | 97.4(1) | O(1)−Ru(1)−N(3) | 91.1(1) |
| O(1)−Ru(1)−N(4) | 171.9(1) | O(1)−Ru(1)−C(1) | 88.4(2) |
| O(1)−Ru(1)−C(2) | 88.7(2) | O(2)−Ru(1)−N(3) | 170.8(1) |
| O(2)−Ru(1)−N(4) | 89.8(1) | O(2)−Ru(1)−C(1) | 90.4(2) |
| O(2)−Ru(1)−C(2) | 90.7(2) | N(3)−Ru(1)−N(4) | 82.0(2) |
| N(3)−Ru(1)−C(1) | 93.3(2) | N(3)−Ru(1)−C(2) | 86.0(2) |
| N(4)−Ru(1)−C(1) | 87.8(2) | N(4)−Ru(1)−C(2) | 95.0(2) |
| C(1)−Ru(1)−C(2) | 176.9(2) | O(3)−Mn(2)−N(2) | 93.9(2) |
| O(3)−Mn(2)−O(4) | 91.9(2) | O(4)−Mn(2)−N(2) | 91.2(2) |
| Ru(1)−C(1)−N(1) | 178.8(4) | Ru(1)−C(2)−N(2) | 175.4(5) |
| Mn(2)−N(2)−C(2) | 168.3(4) | N(2)−Mn(2)−N(2*) | 180.0 |

**Table 4.** Selected Bond Lengths [Å] and Bond Angles [°] for **3**

| | | | |
|---|---|---|---|
| Ru(1)−O(1) | 2.023(5) | Ru(1)−C(7) | 2.046(9) |
| Ru(1)−N(1) | 2.007(7) | Mn(1)−O(2) | 2.29(1) |
| Mn(1)−O(3) | 2.42(2) | Mn(1)−N(2) | 2.213(8) |
| N(2)−C(7) | 1.142(10) | | |
| O(1)−Ru(1)−O(1*) | 97.1(3) | O(1)−Ru(1)−N(1) | 90.9(2) |
| O(1)−Ru(1)−C(7) | 89.9(3) | N(1)−Ru(1)−C(7) | 91.9(3) |
| N(1)−Ru(1)−N(1*) | 81.3(4) | C(7)−Ru(1)−C(7*) | 178.1(4) |
| O(2)−Mn(1)−O(3) | 180.0 | O(2)−Mn(1)−N(2) | 89.5(2) |
| O(3)−Mn(1)−N(2) | 90.5(2) | N(2)−Mn(1)−N(2*) | 179.0(4) |
| Mn(1)−N(2)−C(7) | 164.4(7) | Ru(1)−C(7)−N(2) | 174.7(7) |

**Table 5.** Selected Bond Lengths [Å] and Bond Angles [°] for **4**

| | | | |
|---|---|---|---|
| Ru(1)−O(1) | 2.003(9) | Ru(1)−O(2) | 2.002(9) |
| Ru(1)−O(3) | 2.011(6) | Ru(1)−O(4) | 2.017(6) |
| Ru(1)−C(1) | 2.054(10) | Ru(1)−C(2) | 2.076(9) |
| Ni(1)−N(2) | 2.111(8) | Ni(1)−N(3) | 2.081(9) |
| Ni(1)−N(4) | 2.070(10) | N(1)−C(1) | 1.13(1) |
| N(2)−C(2) | 1.163(10) | | |
| O(1)−Ru(1)−O(2) | 90.9(2) | O(1)−Ru(1)−O(3) | 177.4(2) |
| O(1)−Ru(1)−O(4) | 88.3(2) | O(2)−Ru(1)−O(3) | 89.4(2) |
| O(2)−Ru(1)−O(4) | 178.9(2) | O(3)−Ru(1)−O(4) | 91.5(2) |
| C(1)−Ru(1)−O(1) | 88.6(3) | C(1)−Ru(1)−O(2) | 90.6(3) |
| C(1)−Ru(1)−O(3) | 88.8(3) | C(1)−Ru(1)−O(4) | 90.2(3) |
| C(1)−Ru(1)−C(2) | 177.2(4) | Ru(1)−C(1)−N(1) | 178.7(8) |
| Ru(1)−C(2)−N(2) | 173.1(8) | Ni(1)−N(2)−C(2) | 168.0(8) |
| N(2)−Ni(1)−N(3) | 90.4(3) | N(2)−Ni(1)−N(4) | 88.3(4) |
| N(3)−Ni(1)−N(4) | 84.9(4) | N(2)−Ni(1)−N(2*) | 180.0 |
| N(3)−Ni(1)−N(3*) | 180.0 | N(4)−Ni(1)−N(4*) | 180.0 |

**Table 6.** Selected Bond Lengths [Å] and Bond Angles [°] for **5**

| | | | |
|---|---|---|---|
| Ru(1)−O(1) | 2.003(2) | Ru(1)−O(2) | 2.004(3) |
| Ru(1)−C(1) | 2.067(3) | Co(1)−N(1) | 1.983(2) |
| N(1)−C(1) | 1.145(4) | | |
| O(1)−Ru(1)−O(1*) | 180.0(1) | O(1)−Ru(1)−O(2) | 90.08(10) |
| O(1)−Ru(1)−O(2*) | 89.92(10) | O(1)−Ru(1)−C(1) | 89.5(1) |
| O(1)−Ru(1)−C(1*) | 90.5(1) | O(2)−Ru(1)−O(2*) | 180.0(1) |
| O(2)−Ru(1)−C(1) | 94.6(1) | O(2)−Ru(1)−C(1*) | 85.4(1) |
| C(1)−Ru(1)−C(1*) | 180.0 | N(1)−Co(1)−N(1*) | 121.0(1) |
| N(1)−Co(1)−N(1*) | 104.01(9) | Co(1)−N(1)−C(1) | 171.3(3) |
| Ru(1)−C(1)−N(1) | 174.6(3) | | |

***trans*-$Bu_4N[Ru(Salen)(CN)_2]$ 1.** The $Na^+$ salt of this compound was prepared by the reaction of NaCN with *trans*-[Ru(salen)($PPh_3$)Cl], according to the method of Leung and Che.[10] This was converted to the $Bu_4N^+$ salt by metathesis. The IR spectrum shows a strong $\nu$(C≡N) stretch at 2096 $cm^{-1}$, which is similar to the value of 2099 $cm^{-1}$ in *trans*-$Ph_4P[Ru(acac)_2(CN)_2]$.[8] The structure of **1** has been determined by X-ray crystallography. The ruthenium atom is octahedrally coordinated by the two oxygen atoms and the two nitrogen atoms of the salen ligand and the two carbon


(18) Amsterdam Density Functional (ADF), version 2004.01; *Scientific Computing and Modelling*, *Theoretical Chemistry*; Vrije Universiteit: Amsterdam, 2004.

(19) (a)Wei, H.; Wang, B.; Chen, Z. *Chem. Phys. Lett.* **2005**, *407*, 147−152. (b) Wang, B.; Wei, H.; Wang, W.; Chen, Z. *J. Chem. Phys.* **2005**, *122*, 1−8. (c) Illas, F.; Moreira, I. d. P. R.; Bofill, J. M.; Filatov, M. *Phys. Rev. B* **2004**, *70*, 132414/1−132414/4. (d) Illas, F.; Moreira, I. d. P. R.; de Graaf, C.; Barone, V. *Theor. Chem. Acc.* **2000**, *104*, 265−272.

(20) Hertwig, R. H.; Koch, W. *Chem. Phys. Lett.* **1997**, *268*, 345−351.

(21) Adamo, C.; Barone, V. *J. Chem. Phys.* **1998**, *108*, 664−675.

(22) Perdew, J. P.; Chevary, J. A.; Vosko, S. H.; Jackson, K. A.; Pederson, M. R.; Singh, D. J.; Fiolhais, C. *Phys. Rev. B* **1992**, *46*, 6671−6687.

(23) (a) Noodleman, L. *J. Chem. Phys.* **1981**, *74*, 5737−5743. (b) Noodleman, L.; Baerends, E. J. *J. Am. Chem.* Soc. **1984**, *106*, 2316−2327.

(24) (a) Yan, F.; Chen, Z.-D. *J. Phys. Chem. A* **2000**, *104*, 6295−6300. (b) Dai, D.; Whangbo, M.-H. *J. Chem. Phys.* **2001**, *114*, 2887−2893.

(25) (a) Hu, H.; Chen, Z. *Int. J. Quantum Chem.* **2001**, *88*, 275−279. (b) Hu, H.; Chen, Z.; Liu, C. *Int. J. Quantum Chem.* **2003**, *92*, 428−432. (c) Hu, H.; Yang, X.; Chen, Z. *J. Mol. Struct.* (*THEOCHEM*) **2002**, *618*, 41−46.

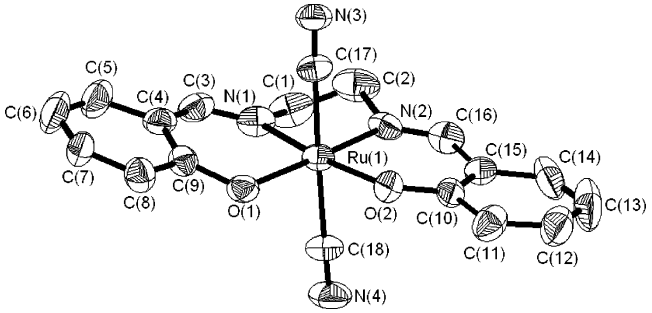


**Figure 1.** ORTEP drawing of [Ru(salen)(CN)$_2$]$^-$ (the anion of **1**) with the atomic numbering scheme.

atoms of the cyanide ions in a trans configuration (Figure 1). The Ru−N and Ru−O distances are similar [2.00(1)−2.03(1) Å]. The average Ru−C (2.07 Å) and C≡N (1.14 Å) distances are essentially the same as that in *trans*-Ph$_4$P[Ru(acac)$_2$(CN)$_2$].

The electrospray ionization mass spectrometry (ESI-MS) of a methanolic solution of **1** (Figure S1, Supporting Information) in the anionic mode shows a peak at $m/z$ = 420, which is due to the parent ion [Ru(salen)(CN)$_2$]$^-$. There is excellent agreement between calculated and experimental isotopic distribution patterns. There is also a minor peak at $m/z$ = 393, which is due to [Ru(salen-H)(CN)]$^-$; this arises from the loss of HCN from the parent ion, most probably as a result of collisions in the lens region.

The cyclic voltammogram of **1** in $CH_3CN$ [0.1 M ($Et_4N$)$BF_4$] has been reported by Leung and Che.[10] It shows two reversible waves at +0.37 and −1.06 V (vs Ag/Ag$^+$), which are assigned to the Ru$^{IV}$/Ru$^{III}$ and the Ru$^{III}$/Ru$^{II}$ couples, respectively. These electrochemical data indicate that [Ru(salen)(CN)]$^-$ is stable with respect to oxidation and reduction.

In summary, similar to *trans*-Ph$_4$P[Ru(acac)$_2$(CN)$_2$], **1** is a very stable species that is soluble in a variety of solvents, and it is therefore a suitable precursor for the construction of ruthenium(III)-containing coordination polymers.

**{Mn(CH$_3$OH)$_4$[Ru(Salen)(CN)$_2$]$_2$}·6CH$_3$OH·2H$_2$O 2.** Reaction of **1** with Mn(acac)$_3$ in refluxing MeOH produces **2** as dark green crystals. The IR shows a $\nu$(C≡N) stretch (2115 cm$^{-1}$) that is shifted to a higher frequency than that in **1**. The structure of **2** has been determined by X-ray crystallography. It is a trinuclear complex, and the Mn$^{II}$ center has a distorted octahedral environment and is coordinated to two [Ru(salen)(CN)$_2$]$^-$ units through the cyano nitrogen atoms and to four methanol molecules in a trans configuration (Figure 2). The bond lengths in the [Ru(salen)(CN)$_2$]$^-$ units [Ru−O 2.011(3), 2.029(3); Ru−N 2.000(4), 2.004(4); Ru−C 2.060(5), 2.061(5); and C≡N 1.143(7), 1.147(7) Å] are essentially the same as in **1**. The Mn−O bond distances [2.191(5)−2.205(4) Å] are slightly longer than the Mn−N distances [2.155(4) Å]. The terminal and bridging Ru−C≡N units are almost linear [178.8(4) and 175.4(5)°, respectively]. The Mn−N≡C units are slightly bent with an angle of 168.3(4)°. The intramolecular Mn···Ru distance is 5.341 Å, the Mn−N−C−Ru torsion angle is 130.08°, and the closest intermolecular Ru···Ru separation is 6.824 Å.

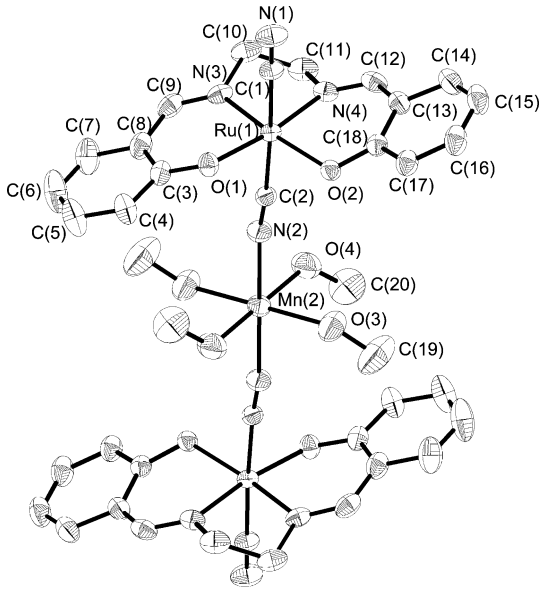


**Figure 2.** ORTEP drawing of {Mn(CH$_3$OH)$_4$[Ru(salen)(CN)$_2$]$_2$}·6CH$_3$OH·2H$_2$O (**2**) with the atomic numbering scheme.

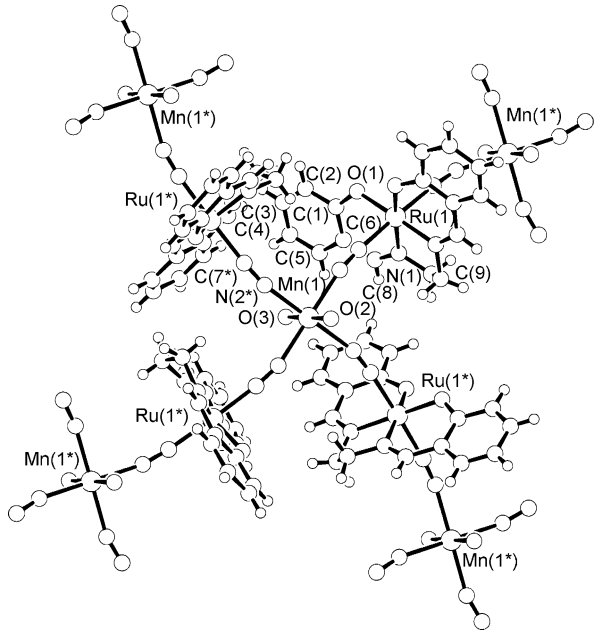


**Figure 3.** View of polymeric {Mn(H$_2$O)$_2$[Ru(salen)(CN)$_2$]$_2$·H$_2$O}$_n$ (**3**) with the atomic numbering scheme.

**{Mn(H$_2$O)$_2$[Ru(Salen)(CN)$_2$]$_2$·H$_2$O}$_n$ 3.** Reaction of **1** with Mn(ClO$_4$)$_2$·6H$_2$O in MeOH at room temperature produces **3** as dark green crystals. The IR shows a $\nu$(C≡N) stretch (2116 cm$^{-1}$) that is the same as in **2** but is shifted to a higher frequency than that in **1**, consistent with the coordination of the cyano nitrogens to Mn$^{II}$. The structure of **3** has been determined by X-ray crystallography. Each Mn$^{II}$ center has a distorted octahedral environment and is coordinated to four [Ru(salen)(CN)$_2$]$^-$ units through the cyano nitrogen atoms in the equatorial positions and to two water molecules in the axial positions (Figure 3). The Mn centers are linked by [Ru(salen)(CN)$_2$]$^-$ to produce a 2-D sheet structure (Figure S3). The bond distances of each [Ru(salen)(CN)$_2$]$^-$ unit in the polymer [Ru−O 2.023(5); Ru−N 2.007(7); Ru−C 2.046(9); and C≡N 1.142(10) Å]

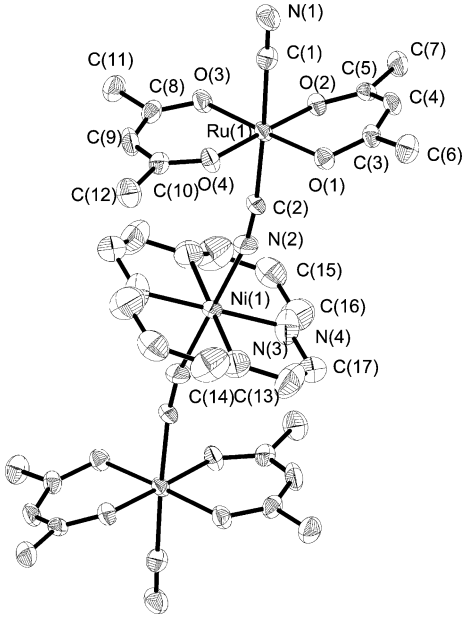


**Figure 4.** ORTEP drawing of $\{Ni(cyclam)[Ru(acac)_2(CN)_2]_2\}\cdot 2CH_3OH\cdot 2H_2O$ (**4**) with the atomic numbering scheme.

are essentially the same as in **1** and **2**. The Mn−N≡C unit is bent with an angle of 164.4(7)°, and the Mn−N−C−Ru torsion angle is 13.75°. The two Mn−$OH_2$ distances [2.29(1) and 2.42(2) Å] are not equivalent. The intralayer Mn···Ru distance is 5.328 Å, the interlayer Mn···Ru distances are 9.675 and 10.469 Å, and the closest interlayer Ru···Ru separation is 8.557 Å.

**$\{Ni(Cyclam)[Ru(Acac)_2(CN)_2]_2\}\cdot 2CH_3OH\cdot 2H_2O$ 4.** Treatment of $NiCl_2\cdot 6H_2O$ and cyclam with *trans*-$Ph_4P[Ru(acac)_2(CN)_2]$ in methanol at room temperature gives compound **4**. The X-ray structure of **4** shows that it is a trinuclear complex (Figure 4) that consists of a $[Ni(cyclam)]^{2+}$ unit bonded to two $[Ru(acac)_2(CN)_2]^-$ ions through the cyano nitrogens. The $Ni^{II}$ center has a distorted octahedral environment and is coordinated to the four nitrogens of the cyclam ligand and to two $[Ru(acac)_2(CN)_2]^-$ units through the cyano nitrogens in a trans configuration. The Ni−N(≡C) distance [2.111(8) Å] is slightly longer than the Ni−N(cyclam) distances [2.070(10) and 2.081(9) Å]. The terminal and bridging Ru−C≡N angles are 178.7(8) and 173.1(8)°, respectively. The bond distances in each $[Ru(acac)_2(CN)_2]^-$ unit [Ru−O 2.002(9)−2.017(6) Å; Ru−C 2.054(10)−2.076(9) Å; and C−N 1.13(1)−1.163(10) Å] are similar to those found in *trans*-$Ph_4P[Ru(acac)_2(CN)_2]$. The intramolecular Ni···Ru distance is 5.293 Å, the Ni−N−C−Ru torsion angle is 163.25°, and the closest intermolecular Ru···Ru separation is 7.622 Å.

**$\{Co[Ru(Acac)_2(CN)_2]_2\}_n$ 5.** Reaction of *trans*-$Ph_4P[Ru(acac)_2(CN)_2]$ with $CoCl_2\cdot 6H_2O$ in MeOH produces **5** as dark purple crystals. The structure of **5** has been determined by X-ray crystallography (Figure 5a). It has a 3-D 2-fold penetrating diamond-like structure (Figure 5b) that is isostructural with $\{Mn[Ru(acac)_2(CN)_2]_2\}_n$.[8] Each $Co^{II}$ center is tetrahedrally coordinated to four $[Ru(acac)_2(CN)_2]^-$ through the cyano nitrogens to produce a 3-D diamond-like structure. The bond lengths and angles [Co(1)−N(1) 1.983(2) Å, Co(1)−N(1)−C(1) 171.3(3)°, and N(1)−Co(1)−N(1*) 104.01(9) and 121.0(1)°] are similar to that in $\{Mn[Ru(acac)_2(CN)_2]_2\}_n$. The bond lengths and bond angles in each $[Ru(acac)_2(CN)_2]^-$ unit in **5** [Ru−O 2.003(2)−2.004(3) Å; Ru−C 2.067(3) Å; C−N 1.145(4) Å; and Ru(1)−C(1)−N(1) 174.6(3)°] are also essentially the same as in the Mn analogue. The Co···Ru distance is 5.173 Å.

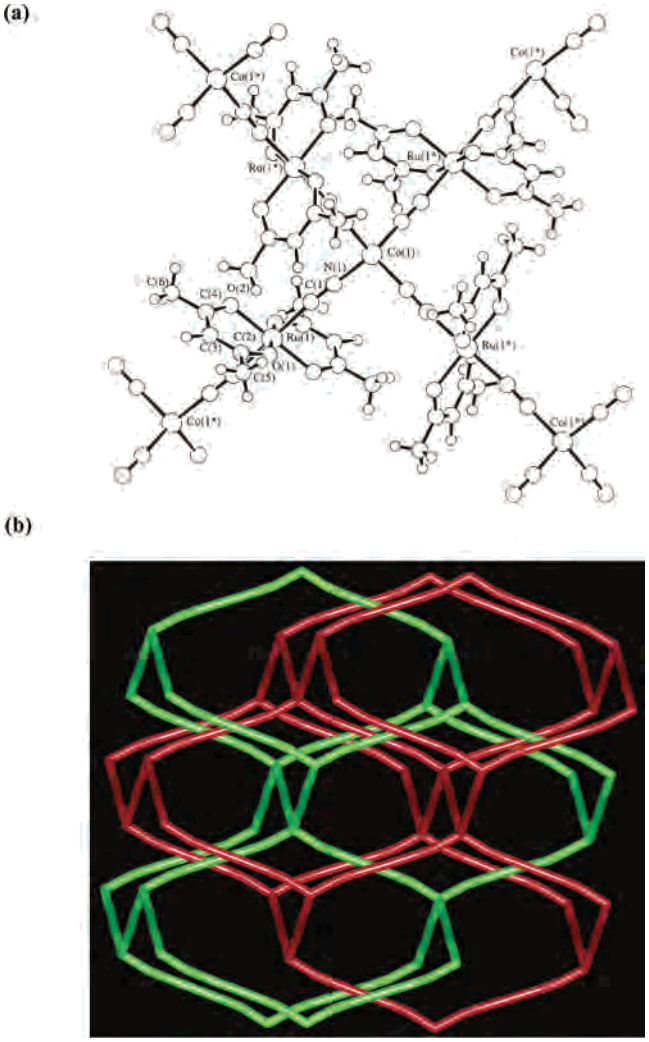


**Figure 5.** (a) View of polymeric $\{Co[Ru(acac)_2(CN)_2]_2\}_n$ (**5**) with the atomic numbering scheme. (b) Two-fold interpenetrating diamond-like networks with Co ions as nodes.

**Magnetic Properties.** The molar magnetic susceptibility data of compound **1** (Figure S5) indicate an unusually strong temperature-independent Van Vleck paramagnetism (TIP) of $2.82 \times 10^{-3}$ cm$^3$ mol$^{-1}$. After subtracting this TIP value, the data obey the Curie−Weiss law [$\chi_m = C/(T - \theta)$] in the temperature range of 2−300 K, with $C = 0.414(1)$ cm$^3$ mol$^{-1}$ K and $\theta = -0.5(2)$ K (Figure 6a). The $C$ value is comparable to that of *trans*-$Ph_4P[Ru(acac)_2(CN)_2]$[8] (0.46 cm$^3$ mol$^{-1}$ K) and is consistent with a low-spin $(t_{2g})^5$ configuration with $S = 1/2$. The field dependence of **1** at 2.0 K is shown in Figure 6b, and the magnetization at 50 kOe is 0.95 N$\beta$ mol$^{-1}$, close to the expected saturation value for a $S = 1/2$ state with $g = 2.0$.

The molar magnetic susceptibility of compound **2** in the temperature range of 20−300 K obeys the Curie−Weiss law [$\chi_m = C/(T - \theta)$], with $C = 6.035(1)$ cm$^3$ mol$^{-1}$ K and $\theta =$

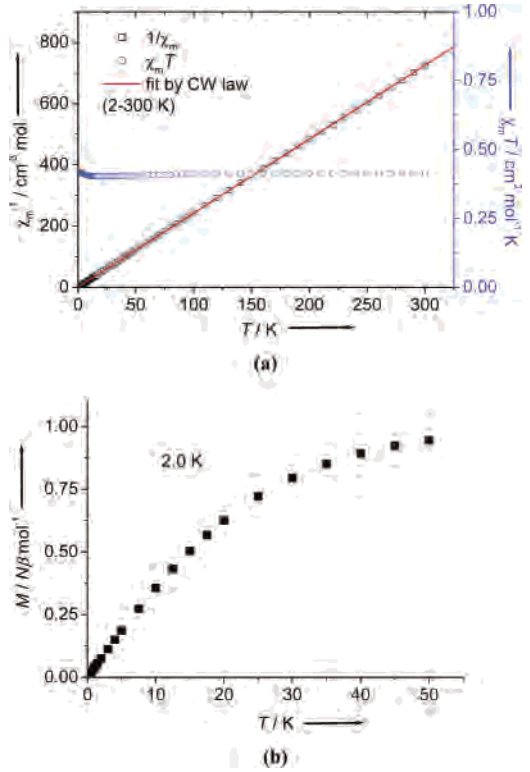


**Figure 6.** (a) Temperature dependence of $\chi_m^{-1}$ and $\chi_m T$ vs $T$ for $Bu_4N$-[Ru(salen)(CN)$_2$] (**1**) measured at 1 kOe. The sample shows a strong temperature-independent paramagnetism (TIP) at $2.82 \times 10^{-3}$ cm$^3$ mol$^{-1}$, which was subtracted in the figure. (b) Field dependence of magnetization of **1** at 2.0 K.

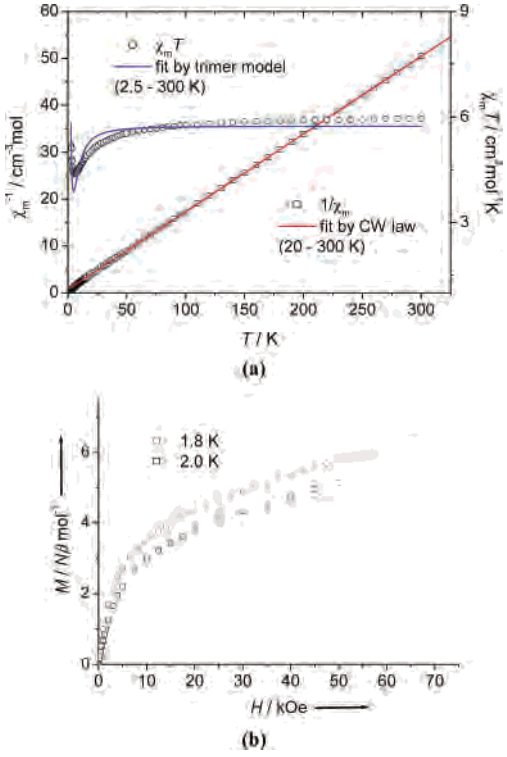


**Figure 7.** (a) Temperature dependence of $\chi_m^{-1}$ vs $T$ for {Mn(CH$_3$OH)$_4$-[Ru(salen)(CN)$_2$]$_2$}·6CH$_3$OH·2H$_2$O **(2)**, exp. (□) and fit (line) using the Curie−Weiss law, and temperature dependence of $\chi_m T$, exp. (○) and fit (line), using the trimer $MnRu_2$ model. (b) Field dependence of magnetization of **2** at 1.8 and 2.0 K.

−4.4(1) K (Figure 7a). The negative $\theta$ value suggests a possible small antiferromagnetic coupling between Ru$^{III}$ and Mn$^{II}$ in **2**. On lowering the temperature, the $\chi_m T$ value decreases gradually and reaches a minimum at about 7 K (4.41 cm$^3$ mol$^{-1}$ K); it then increases abruptly, suggesting a ferrimagnetic-like behavior. The field dependence of the magnetization for **2** was measured at 1.8 and 2.0 K (Figure 7b). The magnetization of this compound per [$MnRu_2$] unit reaches a value of 6.56 N$\beta$ mol$^{-1}$ at 1.8 K and 70 kOe, which is close to the expected value of 7.0 N$\beta$ for the sum of two Ru$^{III}$ and one Mn$^{II}$ magnetic moments ($S_T = 2S_{Ru} + S_{Mn} = 7/2$; $M_s = gS_T N\beta$), suggesting that the antiferromagnetic interaction between Ru and Mn centers is quite weak and that the magnetic moments can be aligned in the direction of the applied field when it is large enough at low temperature. On the basis of the crystal data of **2**, we can assume that the magnetic interaction between Ru ions can be neglected due to their large separation. Thus, the appropriate Hamiltonian for the linear trimer would be $H = -2J(S_{Mn}S_{Ru1} + S_{Mn}S_{Ru2})$, where $J$ is the coupling constant through the cyano bridges. The data are fitted to a linear trimer model using Kambe's method[26] and considering the intertrimer interaction $zJ'$ as a molecular field approach, and the following results are obtained: $J = -1.8(1)$ cm$^{-1}$, $zJ' = 0.87$ (2) cm$^{-1}$ ($z = 6$), $g = 2.117(8)$, and $R = 2.2 \times 10^{-3}$ $\{R = \sum[(\chi_m T)_{obs} - (\chi_m T)_{calc}]^2/\sum(\chi_m T)_{obs}^2\}$. The antiferromagnetic (AF) coupling between Ru(III) and Mn(II) is slightly larger than that ($J_{Fe-Mn} = -0.44$ cm$^{-1}$) observed in the cyano-bridged trimer Mn$^{II}$−Fe$^{III}$−Mn$^{II}$.[27] The ferrimagnetic-like character could arise from the competition between intratrimer−AF and intertrimer ferromagnetic couplings.

The molar magnetic susceptibility of compound **3** in the temperature range of 20−300 K obeys the Curie−Weiss law with $C = 5.157(4)$ cm$^3$ mol$^{-1}$ K and $\theta = -8.33(6)$ K (Figure 8a). The negative $\theta$ value suggests the presence of antiferromagnetic coupling between Ru$^{III}$ and Mn$^{II}$ in **3**. Upon cooling, the $\chi_m T$ value decreases gradually, and the data measured at low field (100 Oe) display a minimum (4.20 cm$^3$ mol$^{-1}$ K) at ca. 36 K. $\chi_m T$ then increases again, suggesting a ferrimagnetic-like character. It could arise from the competition between intralayer−AF and interlayer ferromagnetic couplings. A high magnetic field might remove the anomaly around 36 K. The somewhat larger Weiss constant and the higher temperature for minimum $\chi_m T$ suggest a slightly larger antiferromagnetic interaction between Mn and Ru ions in this compound than in **2**. The magnetization of this compound per [$MnRu_2$] unit reaches only a value of 3.70 N$\beta$ mol$^{-1}$ at 2.0 K and 50 kOe (Figure 8b), which is quite far from the expected value of 7.0 N$\beta$ for the sum of two Ru$^{III}$ and one Mn$^{II}$ magnetic moments ($S_T = 2S_{Ru} + S_{Mn} = 7/2$; $M_s = gS_T N\beta$) but is close to the value of 3.0 N$\beta$ for $S_T = S_{Mn} - 2S_{Ru} = 3/2$, again suggesting that the antiferromagnetic interaction between Ru and Mn centers is stronger in **3** than in **2**.

(26) Kambe, K. *J. Phys. Soc. Jpn.* **1950**, *5*, 48.

(27) Lescouezec, R.; Lloret, F.; Julve, M.; Vaissermann, J.; Verdaguer, M. *Inorg. Chem.* **2002**, *41*, 818−826.

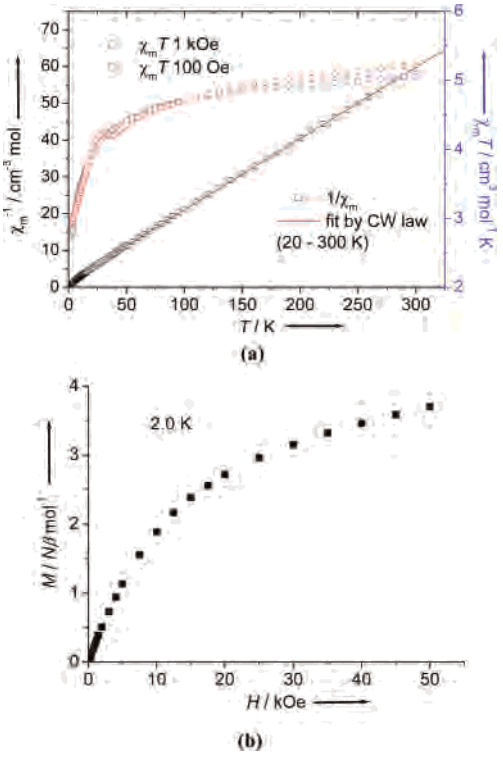


**Figure 8.** (a) Temperature dependence of $\chi_m^{-1}$ vs $T$ for $\{Mn(H_2O)_2[Ru(salen)(CN)_2]_2 \cdot H_2O\}_n$ (**3**), exp. (□) and fit (line) using the Curie−Weiss law, and temperature dependence of $\chi_m T$ measured at 1 kOe and 100 Oe (blue and red ○). (b) Field dependence of magnetization of **3** at 2.0 K.

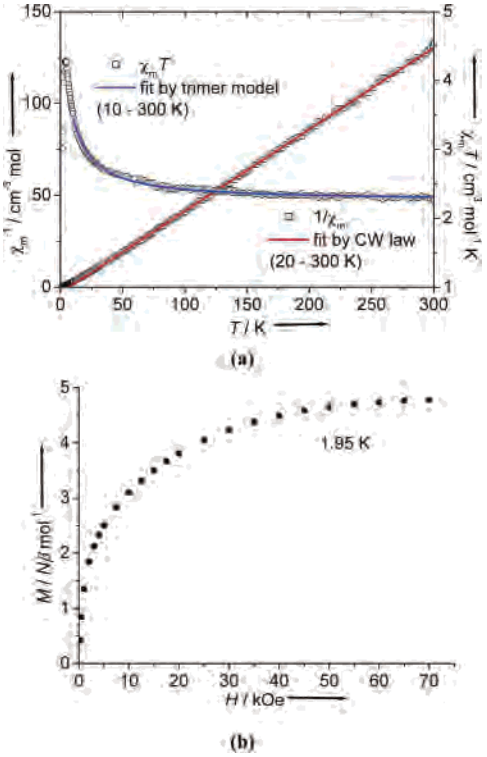


**Figure 9.** (a) Temperature dependence of $\chi_m^{-1}$ vs $T$ for $\{Ni(cyclam)[Ru(acac)_2(CN)_2]_2\} \cdot 2CH_3OH \cdot 2H_2O$ (**4**), exp. (□) and fit (line) using the Curie−Weiss law, and temperature dependence of $\chi_m T$ measured at 10 kOe, exp. (○) and fit (line) using the trimer $NiRu_2$ model. (b) Field dependence of magnetization of **4** at 1.95 K.

The molar magnetic susceptibility of **4** in the temperature range of 20−300 K obeys the Curie−Weiss law with $C = 2.246(6)$ cm$^3$ mol$^{-1}$ K and $\theta = +7.0(1)$ K (Figure 9a). The positive $\theta$ value suggests the presence of ferromagnetic coupling between $Ru^{III}$ and $Ni^{II}$ in **4** through the cyanide bridge. The $C$ value is slightly larger than the uncoupled, spin-only value of 1.75 cm$^3$ mol$^{-1}$ K for one high-spin $d^8$ $Ni^{II}$ center in an octahedral environment with $S = 1$ and two low-spin $d^5$ $Ru^{III}$ centers in an octahedral environment with $S = 1/2$. As the temperature is lowered from 300 K, $\chi_m T$ increases smoothly. Below 50 K, $\chi_m T$ increases abruptly, and it reaches a maximum value of 4.28 cm$^3$ mol$^{-1}$ K at 3.9 K, indicating a ferromagnetic interaction between Ni and Ru centers. By fitting the data above 10 K using a linear Ru−Ni−Ru trimer model developed by Kambe,[26] with $H = -2J(S_{Ni}S_{Ru1} + S_{Ni}S_{Ru2})$, the following parameters are obtained: $J = +4.6(2)$ cm$^{-1}$, $zJ' = 0.02$ (1), $g = 2.269(2)$, and $R = 8.2 \times 10^{-5}$. The magnetization of this compound per $[NiRu_2]$ unit reaches a value of 4.78 N$\beta$ mol$^{-1}$ at 1.95 K and 50 kOe (Figure 9b), which is slightly larger than the expected value of 4.0 N$\beta$ for the sum of two $Ru^{III}$ and one $Ni^{II}$ magnetic moments ($S_T = 2S_{Ru} + S_{Ni} = 2$; $M_s = gS_T N\beta$), again suggesting ferromagnetic interaction between Ru and the Ni centers in **4**. In the temperature dependence of zero-DC field AC magnetic susceptibilities of **4** (Figure S6), the in-phase component ($\chi'_m$) has no maximum down to 2 K, while the out-of-phase component ($\chi''_m$) stays at zero, indicating that no magnetic ordering occurs down to 2 K.

The temperature dependence of $\chi_m T$ for compound **5** is shown in Figure 10a. The $\chi_m T$ value at 298 K is 3.78 cm$^3$ mol$^{-1}$ K, which is larger than the uncoupled, spin-only value of 2.62 cm$^3$ mol$^{-1}$ K for one high-spin $d^7$ $Co^{II}$ center in an tetrahedral environment with $S = 3/2$ and two low-spin $d^5$ $Ru^{III}$ centers in an octahedral environment with $S = 1/2$; this should be mainly due to orbital contributions of the metal ions. As the temperature is lowered, $\chi_m T$ remains almost constant down to ca. 50 K, and it then increases abruptly and reaches a maximum value of 11.1 cm$^3$ mol$^{-1}$ K at ca. 6.4 K; this is much larger than the coupled spin-only value ($S_T$) of 4.375 cm$^3$ mol$^{-1}$ K resulting from the ferromagnetic coupling of one high-spin $Co^{II}$ ($S = 3/2$, $g = 2$) and two low-spin $Ru^{III}$ ions ($S = 1/2$, $g = 2$), suggesting a long-range ferromagnetic ordering. The onset of a long-range magnetic phase transition of compound **5** is evidenced by the low-field temperature dependence of the magnetization shown in Figure 11a, in which the magnetization value increases abruptly below 6 K, characteristic of a long-range magnetic ordering. The ferromagnetic ordering temperature $T_c = 4.6$ K is determined from the maximum of $\chi'_m$ as shown in Figure 11b, where $\chi'_m$ and $\chi''_m$ are the in-phase and out-of phase alternating current (AC) susceptibility, respectively, measured at zero external magnetic field and at an oscillating field frequency range of 111−1111 Hz. No frequency dependence was observed, and this rules out the presence of glassy behavior. However, a small shoulder at around 5.6 K was observed in low-field DC and AC $\chi_m - T$ curves, and it disappears above 300 Oe (Figure 11a). This might be another ferromagnetic transition or just due to trace impurities. The field dependence of the magnetization for **5**

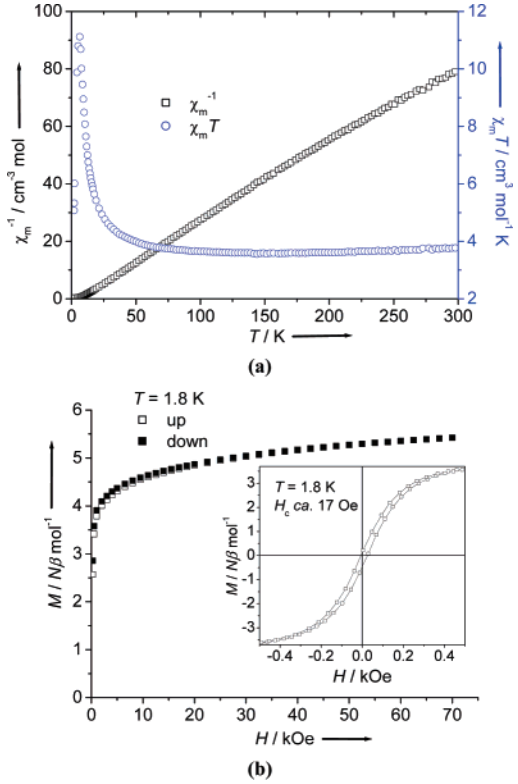


**Figure 10.** (a) Temperature dependence of $\chi_m^{-1}$ (□) and $\chi_m T$ (○) for {Co[Ru(acac)$_2$(CN)$_2$]$_2$}$_n$ (**5**) measured at 10 kOe. (b) Magnetization vs field up to $H = 70$ kOe for **5** at 1.8 K. Inset, hysteresis loop in the ±0.5 kOe range at 1.8 K for **5**, with a coercive field $H_c$ of about 17 Oe.

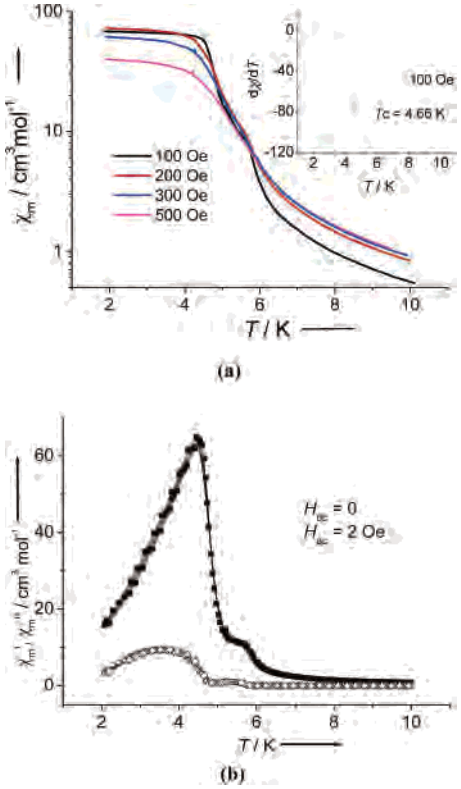


**Figure 11.** (a) Temperature dependence of magnetic susceptibility for **5** measured at low field. (b) Temperature dependence of AC susceptibility for **5** measured at zero external magnetic field and $H_{ac} = 2$ Oe with different frequency 111 Hz (■), 199 Hz (●), 355 Hz (▲), 633 Hz (▼), and 1111 Hz (◆) and in phase $\chi_m'$ (filled symbols) and out-of-phase $\chi_m''$ (open symbols).

was measured at 1.8 K (Figure 10b). The magnetization of this compound increases very rapidly in low field, as expected for a magnet, and reaches a saturation value of $M_s = 5.2$ N$\beta$ at 70 kOe, which is very close to the expected value of 5.0 N$\beta$ for a parallel alignment of two Ru$^{III}$ and one Co$^{II}$ magnetic moments ($S_T = 2S_{Ru} + S_{Co} = 5/2$; $M_s = gS_T N\beta$), further suggesting ferromagnetic coupling between the Ru and the Co centers. A characteristic hysteresis loop is observed for **5** at 1.8 K (inset of Figure 10b) with a coercive field of ca. 17 Oe, which is slightly larger than that in the Mn analogue (ca. 6 Oe), presumably due to the stronger anisotropy of the Co$^{II}$ ion.

**DFT Calculations of Superexchange Interaction. Magnetic Orbital Analysis.** From the single determinant calculation in ADF,[18] the singly occupied molecular orbitals in the highest spin state for the system considered can be obtained. These orbitals are often called molecular magnetic orbitals, which are composed of the local magnetic orbitals located on each paramagnetic center. On the other hand, on the basis of calculations on the antiferromagnetic configuration by using the broken symmetry approach,[23] the local magnetic orbitals can also be obtained, which describe the distribution of the active spin electrons on each local magnetic center. Besides the paramagnetic metal ion, these local magnetic orbitals contain possible components of bridging and/or terminal ligands. An analysis of molecular magnetic orbitals should provide insight into the nature of the Ru−M superexchange interaction.

As shown by X-ray crystallography, the Ru$^{III}$, Mn$^{II}$, and Ni$^{II}$ ions in compounds **2** and **4** are all in a distorted octahedral environment. For simplicity, the distortion from the octahedral coordination was ignored. At this approximation, the symmetry of the local magnetic orbitals with metal d-character is shown in Scheme 1. It is found that in the Ru$^{III}$-containing fragment of compounds **2** and **4**, only one local magnetic orbital is predominantly located on the d-orbital with $t_{2g}$ site-symmetry for the low-spin Ru$^{III}$ ion (i.e., the $d_{xz}$-orbital). On the other hand, the five local magnetic orbitals of the Mn$^{II}$-containing fragment in **2** are predominantly located on the d-orbitals of the high-spin Mn$^{II}$ ion, which have either $e_g$ and $t_{2g}$ site-symmetry. In **4**, the

**Scheme 1**

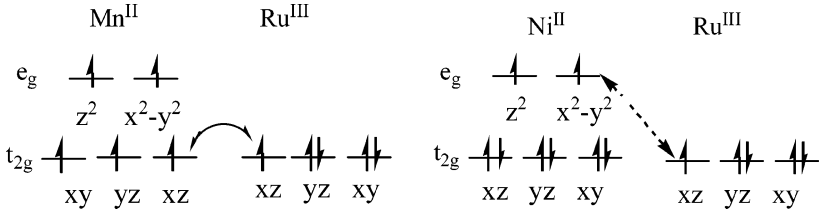

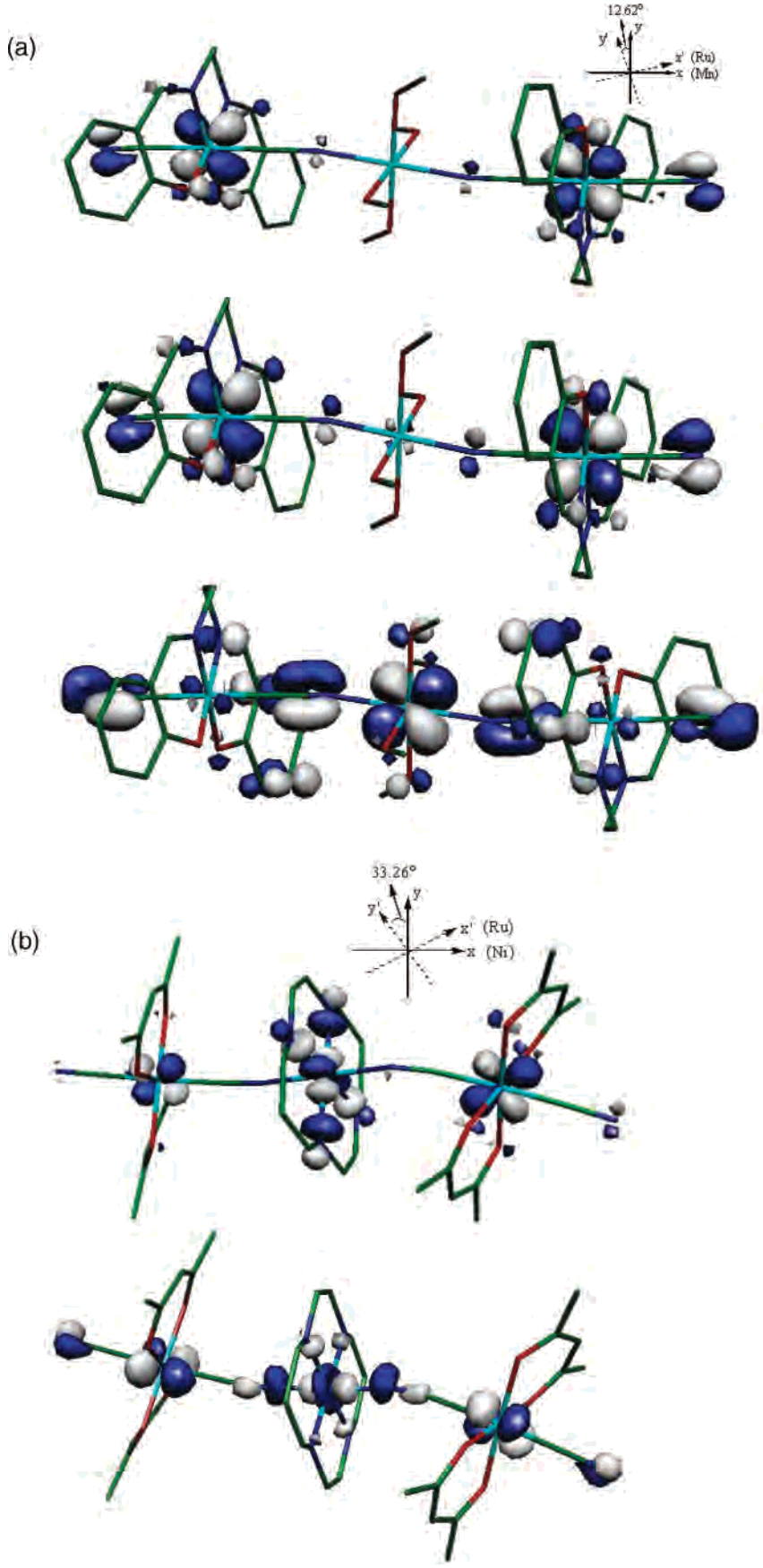


**Figure 12.** Selected molecular magnetic orbitals for (a) Ru−Mn compound **2** and (b) Ru−Ni compound **4**.

two local magnetic orbitals of the $Ni^{II}$-containing fragment are predominantly located on the $d_{z2}$ and $d_{x2-y2}$ orbitals of the high-spin $Ni^{II}$ ion, with $e_g$ site-symmetry. On the basis of symmetry considerations, it is evident that for compound

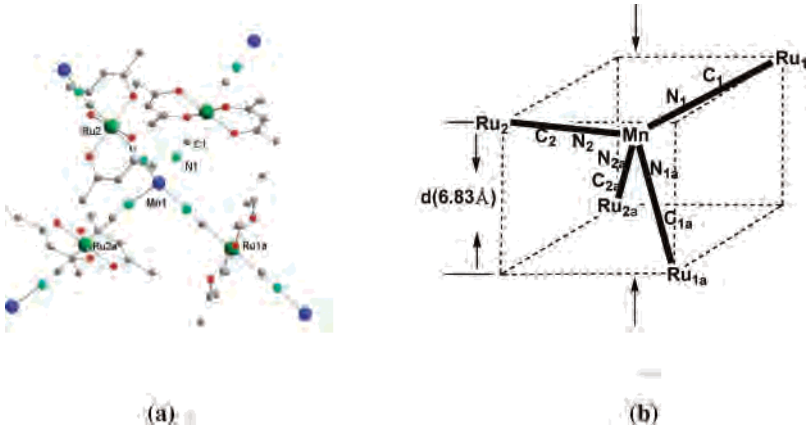


**Figure 13.** Model compound for the 3-D structure of compound **6**: (a) structure scheme and (b) compressed tetrahedron configuration.

**Table 7.** Calculated Exchange Coupling Constants $J$ for $Ru^{III}_2Mn^{II}$ Compounds ($cm^{-1}$)[a]

| compound | **2** | **3** | **6** |
|---|---|---|---|
| $J_{cal}$ | −0.43 | −1.23 | +3.79 |
| $J_{exp}$ | −1.08 | AF | F |

[a] Spin Hamiltonian $H = -2J$ ($S_{Mn}S_{Ru1} + S_{Mn}S_{Ru2}$). AF and F denote antiferromagnetic and ferromagnetic characteristics, respectively.

**2**, the superexchange interaction between $Ru^{III}$- and $Mn^{II}$-containing fragments should be antiferromagnetic, while the superexchange interaction between $Ru^{III}$- and $Ni^{II}$-containing fragments in compound **4** is predicted to be ferromagnetic.

Figure 12 shows selected molecular magnetic orbitals for compounds **2** and **4**. In the case of compound **2**, the molecular magnetic orbitals consist of $d_{xz}$ orbitals on $Ru^{III}$ and $Mn^{II}$, together with a $\pi$-orbital component of the C≡N bridges, resulting in an antiferromagnetic superexchange interaction between $Ru^{III}$ and $Mn^{II}$ ions. In contrast, in compound **4**, the orthogonality of the local magnetic $d_{xz}$ orbital on $Ru^{III}$ and the $d_{x2-y2}$ orbital on $Ni^{II}$ leads to ferromagnetic superexchange interactions between $Ru^{III}$ and $Ni^{II}$ ions. Evidently, these calculated magnetic orbitals can reasonably explain the experimental observations.

**Calculation of Magnetic Coupling Constants.** Through DFT-BS calculations on the highest-spin state and the broken symmetry state, the superexchange coupling constants $J$ can be evaluated. To compare the exchange characteristics between $Ru^{III}$ and $Mn^{II}$ in various structure types, the coupling constants in the trinuclear compound **2**, the 2-D compound **3**, and our previously reported 3-D compound $\{Mn[Ru(acac)_2(CN)_2]\}_n$ (**6**)[8] were calculated by using DFT-BS at the hybrid functional mPW/B3LYP level. These three compounds all have the same $Mn^{II}Ru^{III}_2$ composition. For compound **3**, $\{[Mn(H_2O)_2][Ru(salen)(CN)_2]_4\}$ with a distorted $D_{4h}$ symmetry is taken as the model compound to represent a unit of the 2-D structure. In the case of the 3-D diamond-like compound **6**, the model compound is $\{Mn[Ru(acac)_2(CN)_2]_4\}$ with distorted $T_d$ symmetry (Figure 13a). In our calculations, experimental structural data determined from X-ray crystallography were used.

As in shown Table 7, the calculated coupling constants ($J_{cal}$) are in qualitative agreement with the experimental values ($J_{exp}$). Both trimer **2** and model molecule for the 2-D compound **3** have a negative $J$ value, which indicates antiferromagnetic coupling between $Ru^{III}$ and $Mn^{II}$. On the other hand, the positive $J$ value of the model molecule for the 3-D compound **6** indicates ferromagnetic coupling. As shown experimentally, the antiferromagnetic interactions in compounds **2** and **3** are quite weak. This may be attributed to small overlap integrals between the local magnetic orbitals on $Ru^{III}$ and $Mn^{II}$. The ADF calculated overlap integrals $S$ for compounds **2**, **3**, and **6** are 0.0160, 0.0329, and 0.0000, respectively, which reveal small $S$ values for compounds **2** and **3**. In terms of the orbital interaction theory, these small overlap integrals mean weak antiferromagnetic interactions. On the other hand, in compound **6**, antiferromagnetic interaction is unfavorable due to the relative orientations of the local magnetic orbitals. This accidental orthogonality ($S = 0$) leads to ferromagnetic coupling.

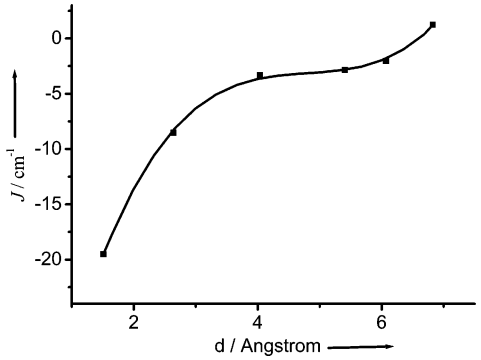


**Figure 14.** Plot of $J_{cal}$ vs $d$ for model compound of **6**.

It is interesting to note that different magnetic interactions occur between the 2-D and the 3-D $Ru^{III}_2Mn^{II}$ compounds. To gain more insight into this magneto-structural relationship, we examined the change in the superexchange interaction between $Ru^{III}$ and $Mn^{II}$ as the geometry of the $MnRu_4$ unit in **6** changes from tetrahedral to planar quadrangle. This is done by calculating the coupling constants at various $d$ values as the tetrahedral $MnRu_4$ unit is compressed (Figure 13b). Figure 14 shows a plot of calculated $J$ values versus $d$. In the starting model unit for **6**, the average experimentally measured $d$ value is 6.83 Å, and $\theta(N_1MnN_2)$ is 103.5°; this gives a calculated $J$ value of +3.79 $cm^{-1}$. As $d$ is decreased, the magnetic exchange interaction gradually changes from ferromagnetic to antiferromagnetic. At $d = 1.51$ Å, $\theta(N_1$-

$MnN_2$) is 180°, and the geometrical configuration becomes an approximate planar quadrangle; the system has a maximum antiferromagnetic interaction with a $J$ value of $-19.52$ $cm^{-1}$. It should be pointed out that this quadrangle configuration is somewhat different from the model compound of **3** because in the latter, the $Ru^{III}$ ion is in octahedral coordination, but the former has a four-coordinate $Ru^{III}$ ion. Moreover, the compressed model compound of **6** with $\theta$-($N_1MnN_2$) of 180° is not an ideal planar quadrangle due to the bent $Mn^{II}-N-C-Ru^{III}$ unit. Nevertheless, this analysis can at least qualitatively explain the change in magnetic behavior as the geometry changes.

## Conclusions

The use of *trans*-$[Ru(acac)_2(CN)_2]^-$ and *trans*-$[Ru(salen)(CN)_2]^-$ as building blocks has produced a number of trinuclear, 2-D, and 3-D $M^{II}Ru^{III}_2$ (M = Mn, Ni, Co) compounds. Studies of the magnetic properties of these compounds indicate antiferromagnetic interaction between Ru and Mn in the trinuclear and 2-D $Mn^{II}Ru^{III}_2$ compounds, ferromagnetic interaction between Ni and Ru in the trinuclear $Ni^{II}Ru^{III}_2$ compound, and long-range ferromagnetic ordering at low temperatures in the 3-D $Co^{II}Ru^{III}_2$ compound. DFT calculations show that the superexchange interaction between $Ru^{III}$ and $M^{II}$ ($Mn^{II}$, $Ni^{II}$) is governed by the electronic configuration of the paramagnetic ions as well as the geometric configuration of the compound.

**Acknowledgment.** This work was supported by a grant from the NSFC/RGC Joint Research Scheme (20318001/9050173) and NSFC Nos. 20125104, 20490210, and 20273005.

**Supporting Information Available:** Additional figures giving crystal packing diagrams, ESI-MS, magnetic susceptibility plots, and X-ray crystallographic files in CIF format for compounds **1**−**5**. This material is available free of charge via the Internet at http://pubs.acs.org.

IC0506456